Nuclear Instruments and Methods in Physics Research A 615 (2010) 333–339

Contents lists available at ScienceDirect

Nuclear Instruments and Methods in Physics Research A

journal homepage: www.elsevier.com/locate/nima

Development of double-scattering-type Compton camera with double-sided silicon strip detectors and NaI(Tl) scintillation detector

Hee Seo [a], Chan Hyeong Kim [a,*], Jin Hyung Park [a], Jong Kyung Kim [a], Ju Hahn Lee [b], Chun Sik Lee [b], Jae Sung Lee [c]

[a] Department of Nuclear Engineering, Hanyang University, 17 Haengdang-dong, Seongdong-gu, Seoul 133-791, Republic of Korea
[b] Department of Physics, Chung-Ang University, 221 Heukseok-dong, Dongjak-gu, Seoul 156-756, Republic of Korea
[c] Department of Nuclear Medicine and Interdisciplinary Program in Radiation Applied Life Science, Seoul National University, 28 Yeongeon-dong, Jongno-gu, Seoul 110-744, Republic of Korea

ARTICLE INFO

Article history:
Received 14 November 2009
Received in revised form
2 February 2010
Accepted 4 February 2010
Available online 10 February 2010

Keywords:
Compton camera
Double-scattering
Double-sided silicon strip detector
NaI(Tl) scintillator

ABSTRACT

In the present study, a double-scattering-type Compton camera, which incorporates two double-sided silicon strip detectors (DSSDs) as the scatterer detectors and an NaI(Tl) detector as the absorber detector, was constructed as a proof-of-principle system for a compact high-imaging-resolution Compton camera. The energy and timing resolutions of the component detectors were determined accurately for effective Compton imaging. Then, the Compton camera was used to image an ^{22}Na point source at 3.7 cm. The imaging resolutions of the current system were 9.0 and 4.8 mm FWHM for 511 and 1275 keV, respectively, which are fairly good considering the limitations of the detectors and data acquisition (DAQ) electronics employed. Given the characteristics of the component detectors, it is believed that the double-scattering Compton camera can be developed as a very compact system (similar in size to a hand-held radiation survey meter) providing very high imaging resolution.

1. Introduction

Since the concept of Compton imaging was first introduced in the 1970s [1], several different types of Compton cameras have been constructed for different applications in fields including astrophysics, nuclear medicine, and molecular imaging, as well as security inspection [2–5]. This imaging technique is based on Compton kinematics-based electronic collimation rather than the mechanical collimation used by most conventional imaging devices, and usually two position-sensitive gamma-ray detectors are employed, as shown in Fig. 1. Images are acquired from so-called "effective events" in which a photon emitted from a radiation source undergoes a Compton scattering in the scatterer detector and then is completely absorbed in the absorber detector. By tracking a single photon, the location of the radiation source in three-dimensional space can be determined to be somewhere on a given conical surface. The vertex and axis of the conical surface are determined by the interaction locations in the scatterer and absorber detectors, while the half-angle (θ) of the cone is calculated according to the energy of the source photon and the deposited energy in one of the detectors, the scatterer or the absorber. If the source energy to be imaged is unknown, one could use the peak energy appearing in the sum-energy spectrum, which can be obtained by the summation of the measured energies in the scatterer and the absorber, as the source energy. The formation of as few as three cones, in principle, can determine the exact location of a point source in three-dimensional space.

Compton imaging has several advantages over the conventional mechanical-collimation-based imaging techniques. First, the location of a radiation source in three-dimensional space, or even the three-dimensional distribution of a radiation source or radioactive contamination, can be determined by a single measurement at a "fixed" position. Compton imaging also provides a wide field-of-view, making possible imaging of very large objects or contaminated areas, such as a building, or even larger areas. Another feature of Compton imaging is multi-tracing capability, which makes it possible to image several different kinds of radioisotopes simultaneously. Compton imaging, in principle, provides much higher imaging sensitivity than conventional mechanical-collimation-based imaging techniques, resulting in significant reductions of imaging time and patients' radiation exposure. Compton imaging also provides better imaging resolution for higher-energy photon sources due to the characteristics of Doppler broadening effect and detector energy resolution. Note that the photon energy can be determined with less uncertainty for a higher-energy photon, resulting in better imaging resolution in a Compton camera. In addition, the imaging

* Corresponding author. Tel.: +82 2 2220 0513; fax: +82 2 2220 4059.
E-mail address: chkim@hanyang.ac.kr (C.H. Kim).

0168-9002/$ - see front matter © 2010 Elsevier B.V. All rights reserved.
doi:10.1016/j.nima.2010.02.060

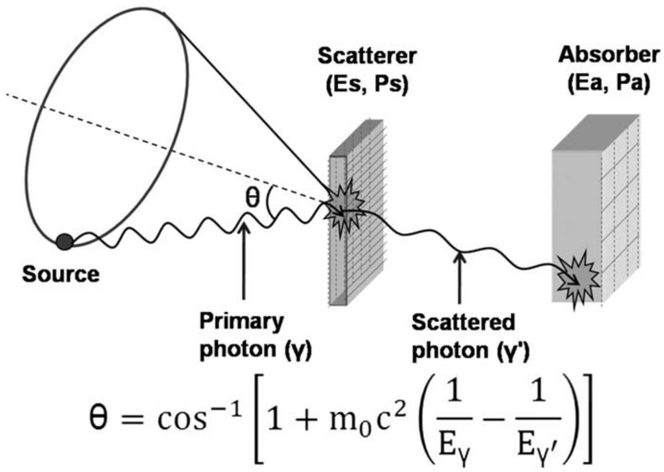

Fig. 1. Concept of Compton imaging. The vertex and axis of the conical surface are determined by the interaction positions in the scatterer and absorber detectors, while the half-angle (θ) of the cone is determined by the energy of the source photon (E_γ) and the deposited energy in one of the detectors, the scatterer or the absorber.

resolution and sensitivity are only weekly linked in Compton imaging.

Typically, single-scattering-type Compton cameras use two plane-type position-sensitive semiconductor detectors, one for the scatterer and the other for the absorber [6–9]. For segmented germanium detectors, which are frequently used as absorber detectors, the segments are relatively large, resulting in low spatial resolution of the absorber detector and, consequently, limited imaging resolution [10]. Si(Li) or germanium strip detectors offer better spatial resolution in the planar direction, but were not considered in the present study, mainly because the method to determine the interaction depth in the detector is still subject to have some uncertainties when the detectors are used in harsh environments or when multiple interactions occur in the same detector for a single gamma trajectory. These detectors also require an additional cooling system, which is obviously disadvantageous to our objective of developing a very compact system. Note that some Compton cameras use several position-sensitive detectors for its scatterer and/or absorber to enhance imaging sensitivity [3,11–13]; normally, several layers of position-sensitive silicon detectors are used for scatterer and one or more of position-sensitive scintillation detectors or semiconductor detectors are used for absorber. It should be, however, noted that these systems are all single-scattering-type Compton cameras because only one scattering position among the scatterer detectors and one absorbing position among the absorber detectors are used in the reconstruction of Compton images.

In the present study, a double-scattering-type Compton camera was constructed as a proof-of-principle system for a compact high-resolution Compton camera, using two position-sensitive semiconductor detectors and an NaI(Tl) scintillation detector. This double-scattering-type Compton camera [14] is the simplest form of a multiple-scattering-type Compton camera [15,16], in which the photon emitted from the gamma source can undergo a multiple number of Compton scatterings in the scatterer detectors before it is fully absorbed in the absorber detector. The purpose of double scattering in the present study was to maximize the imaging resolution by accurately determining the trajectory of a photon between the two high-spatial-resolution scatterer detectors. This type of Compton camera will offer, in principle, a very high imaging resolution, at the expense of imaging sensitivity. Note that silicon, which is a low atomic number material (Z=14), is considered to be the best detector material for the scatterer detectors from the perspective of Doppler broadening, the effect of which frequently is considered to be the theoretical limitation of Compton imaging resolution [17]. Moreover, our double-scattering Compton camera does not require a cooling system, thereby making possible the development of a very compact system.

2. Materials and method

2.1. Prototype system

Fig. 2 shows the current proof-of-principle version of the double-scattering-type Compton camera, which consists of two identical double-sided silicon strip detectors (DSSDs, W1(DS), 50 mm × 50 mm × 1.5 mm; Micron Semiconductor, Sussex, UK) as the scatterer detectors and an NaI(Tl) scintillation detector (Model 905-4, 3 in. diameter × 3 in. height; ORTEC, TN, USA) as the absorber detector. The spatial resolution of the current scatterer detectors is not very high (3 mm × 3 mm × 1.5 mm), but they will be replaced with much higher spatial resolution detectors in the final system. For an effective event, the photon must have Compton scatterings with both of the scatterer detectors in sequence and then be completely absorbed in the absorber

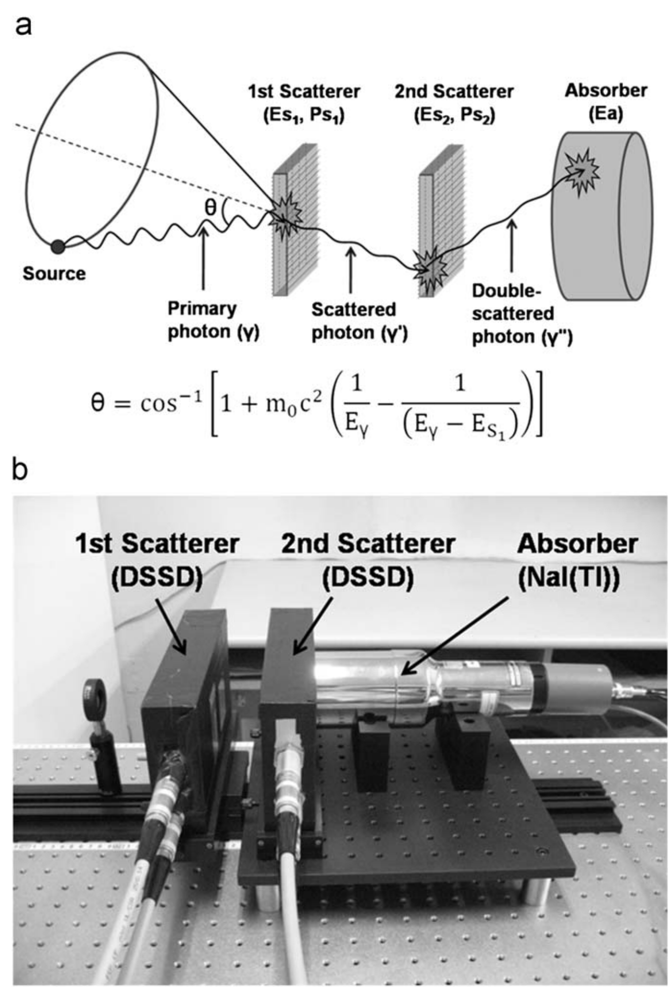

Fig. 2. Principle of double-scattering Compton camera (upper) and prototype double-scattering Compton camera constructed in present study (lower). The Compton camera is composed of two double-sided silicon strip detectors (DSSDs) placed inside of light-impervious aluminum boxes, and an NaI(Tl) scintillation detector.

detector. Using the interaction positions in these high-spatial-resolution scatterer detectors, the track of the scattered photon can be determined very accurately. In the double-scattering Compton camera, the absorber detector is used only for energy gating and coincidence counting and, therefore, a position-sensitive detector is not mandatory. For this reason, a regular NaI(Tl) scintillation detector was used for the absorber detector. The Compton camera is run with an NIM- and CAMAC-based data acquisition (DAQ) system, and the digitized data are analyzed with ROOT-based software specifically developed for the Compton camera [18].

2.2. Determination of energy and timing resolutions

The energy and timing resolutions are very important parameters to be determined for effective energy gating and coincidence counting in Compton imaging. These parameters are also necessary for accurate detector simulations in system optimization. To measure the timing resolution of the NaI(Tl) scintillation detector, two identical NaI(Tl) detectors were connected to identical DAQ electronics (Fig. 3). With the coincidence detection logic for the two detectors, an ^{22}Na check source was placed between the detectors, and two 511 keV annihilation photons, which are emitted at the same time, were measured using them.

The signal extracted from the anode was used for the measurement of the timing resolution, while the signal extracted from the dynode was used for the measurement of the energy resolution. For the timing measurement, the anode signal was fed into the timing filter amplifier (TFA; ORTEC 474, USA) with the differentiation time of 50 ns and the integration time of 20 ns. A constant fraction discriminator (CFD; ORTEC 935, USA) was used for the time pick-off. The logic signal generated from the CFD was split into two gate and delay generators in the octal gate and delay generator (GDG; ORTEC GG8020, USA), after which, one was fed into the coincidence logic and the other was fed into the time-to-digital convertor (TDC; Phillips Scientific 7186, USA) as a stop signal. If the two signals from the NaI(Tl) scintillation detectors are within a coincidence window of 100 ns, the coincidence signal is generated, and is fed into the TDC as a common start signal, and into the peak-sensing analog-to-digital convertor (ADC; Phillips Scientific 7164, USA) as a gate signal. The other channel of the coincidence signal is delayed by 30 μs and fed into the look-at-me generator (LAM; Kaizu Works, Japan) to secure sufficient time to digitize an analog signal in the digitizer (ADC and TDC). For the energy measurement, the dynode signal was processed in the preamplifier (ORTEC 276, USA) and the spectroscopic amplifier (ORTEC 572A, USA) with the shaping time of 2 μs. The Gaussian-shaped linear signal was then digitized in the ADC only when the gate was open. To record exclusively the coincidence event generated by the annihilation photons, the energies deposited in the detectors were recorded in a data file and an off-line energy gate ($=511\pm50$ keV) was applied to the measured data.

Due to the low efficiency for full-energy absorption event of 511 keV photons in the DSSD, the method used for measuring the timing resolution of the NaI(Tl) detector was inappropriate. Therefore, a scattering geometry with an NaI(Tl) detector placed directly behind the DSSD (Fig. 4) was used to determine the timing resolution of the DSSD for the 662 keV ^{137}Cs source. Considering that the timing resolution of the DSSD and related electronics is expected to be a few tens of ns, the use of the scattering geometry would not significantly affect the time difference distribution. Fig. 5 shows the DAQ logic, which is very similar to that of the NaI(Tl) detector except for the DSSD trigger part.

The MUX-16 (mesytec GmbH & Co., Germany) is utilized to handle 16-channel signals from one side of the DSSD; hence, in the present study, two MUX-16 s were employed for DSSD signal

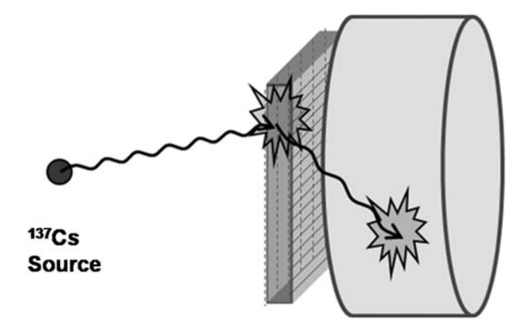

Fig. 4. Scattering geometry with DSSD and NaI(Tl) detectors. The ^{137}Cs source was placed 4 cm in front of the DSSD, and the distance between the two detectors was 1 cm.

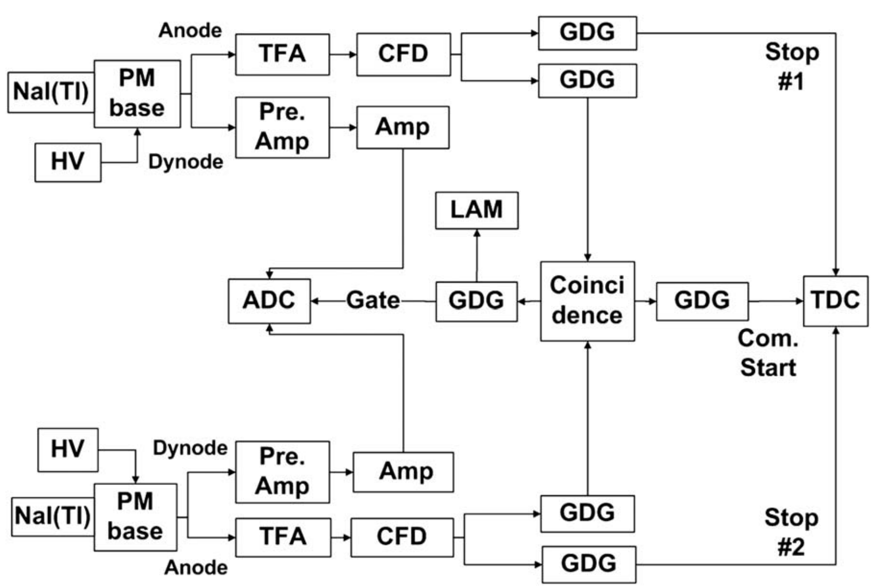

Fig. 3. Block diagram of data acquisition (DAQ) electronics for measurement of timing resolution of NaI(Tl) scintillation detector with coincidence logic.

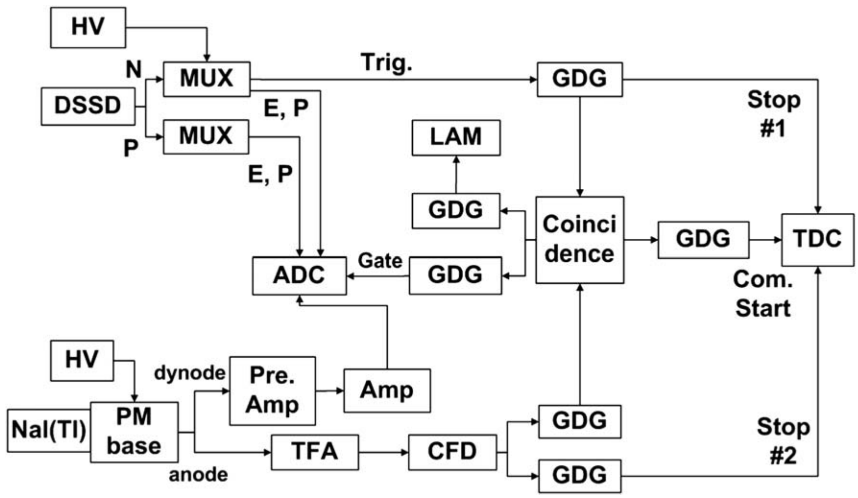

Fig. 5. Block diagram of data acquisition (DAQ) electronics to determine timing resolution of DSSD with coincidence logic.

processing. The MUX-16 has a multiplexing capability for 16 channels of input signal, and up to two output signals occurring within 50 ns can be processed. In the MUX-16, the preamplified signal is split and fed into the shaping amplifier and the leading-edge discriminator. The output signals from the MUX-16 are linear signals for energy (E) and position (P) information, and a negative NIM logic signal for time information. In order to consider only 662 keV photons from the ^{137}Cs check source, the energy deposited in the detectors was again recorded, and a sum energy gate (=662 $\pm$ 60 keV) was applied to the data.

2.3. Image acquisition and analysis

The double-scattering Compton camera was used to image a point source. Preparatory to this, the distance between the first and second scatterer detectors was set at 10 cm. The absorber detector was placed 1 cm behind the second scatterer detector. A point-like (1 mm diameter) ^{22}Na check source (281 kBq), which emits low-energy positrons (resulting in 511 keV annihilation photons) and 1275 keV gamma-rays, was placed 3.7 cm from the camera. The maximum scattering angle that was measurable with the current experimental setup was about 80°, which was limited by the detection geometry between the gamma source and the component detectors, while the minimum scattering angle was limited by the energy discrimination level of the first scatterer detector. After acquiring a sufficient number of effective events, the image was reconstructed using a list-mode maximum-likelihood expectation-maximization (ML-EM) algorithm [19,20]. In the ML-EM algorithm, the system matrix represents the probability that a photon emitted from a voxel in a three-dimensional image space is recorded as the effective event mentioned earlier. The system matrix used in the present study was factorized into two parts; that is, (1) the probability that the photon scatters in an angle ω, and (2) the probability that the voxel belongs to a conical surface determined from the two interaction positions in each scatterer detector and the scattering angle ω. To calculate the probability of (1), the Klein–Nishina formula with the assumption of an unbounded electron at rest was used. To calculate the probability of (2), the ray-tracing method, in which the probability is determined by the intersecting chord length of a line on a conical surface within the voxel, was used [21]. Neither energy uncertainty nor Doppler broadening was considered in the reconstruction algorithm. The number of iterations was 7. The camera's imaging resolution was determined in terms of the full-width-at-half-maximum (FWHM) for a point source.

The performance of the Compton camera was evaluated also with reference to the angular resolution measure (ARM) [17]. The ARM, which represents the minimal angular distance between the reconstructed circle and the known source location [22], was calculated as follows:

$$\Delta\theta = \theta_{\text{geometry}} - \theta_{\text{energy}} \tag{1}$$

where $\Delta\theta$ is the ARM, θ_{geometry} the scattering angle determined from the known source position and the interaction positions in the component detectors, and θ_{energy} the scattering angle determined from the deposited energies in the component detectors and the Compton scattering formula. The ARM is affected by the spatial and energy resolutions of the component detectors as well as by Doppler broadening in Compton scattering. Note that the ARM distribution reflects only the performance of the Compton imaging system, not the performance of the image reconstruction algorithm. From the ARM distribution, one can determine the angular resolution of the Compton camera after fitting the distribution. Because the ARM distributions have long tails, the Voigt function, which is a convolution of the Gaussian distribution and the Lorentzian distribution, was used to fit the ARM distributions [23]. The FWHM of the Voigt function can be calculated as follows [24]:

$$\text{FWHM} \approx 0.5346 f_L + \sqrt{0.2169 f_L^2 + f_G^2} \tag{2}$$

where f_L and f_G are the FWHM of the Lorentzian and Gaussian distributions, respectively.

3. Results and discussion

3.1. Energy and timing resolutions of component detectors

The energy resolution of the scatterer detectors was determined to be of the order of ~20 keV for the deposited energies of interest (50–300 keV). The resolution was mostly system resolution, which represents the broadening effects of the electronic components after each detector. The energy resolution of the absorber detector was estimated to be ~8% for the scattered photon energies of interest (300–1000 keV). It was 6.6% and 5.8% for the ^{60}Co 1173 and 1332 keV peaks, respectively. Considering the energy resolution of the component detectors, the energy window for energy gating was set at $\pm$10% of the source energy, that is, 511 ± 51 and 1275 ± 127 keV for the 511 and 1275 keV gammas, respectively.

Fig. 6 shows the time difference distribution between the two NaI(Tl) detectors. The coincidence timing resolution of the detectors was determined to be 10.97 ns FWHM after applying the 511 keV energy gate. Under the assumption that the detectors have the same timing properties, the timing resolution of each NaI(Tl) detector and related electronics was found to be 7.76 ns from the following equation, where x is the timing resolution of the NaI(Tl) scintillation detector.

$$10.97\ \mathrm{ns} = \sqrt{x^2 + x^2} \tag{3}$$

The coincidence timing resolution of the combination of the DSSD and the NaI(Tl) detector was determined to be 57.97 ns FWHM from the time difference distribution (Fig. 7). Considering the timing resolution of the NaI(Tl) scintillation detector, the timing resolution of the DSSD and related electronics was found to be 57.45 ns from the following equation, where x is the timing resolution of the DSSD and y is the timing resolution of the NaI(Tl) scintillation detector (=7.76 ns).

$$57.97\ \mathrm{ns} = \sqrt{x^2 + y^2} \tag{4}$$

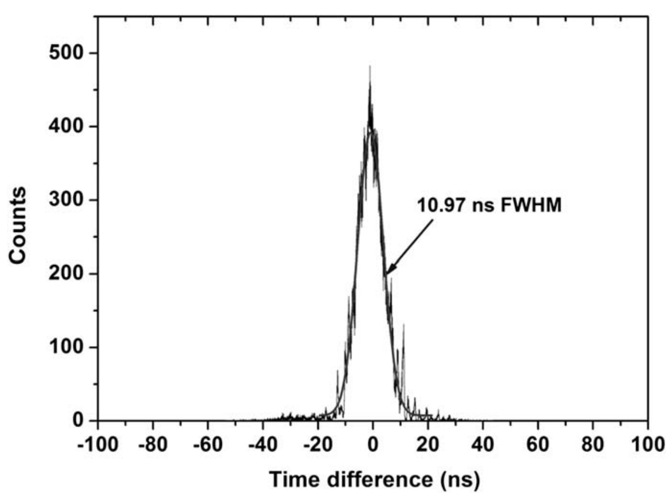

Fig. 6. Time difference distribution between two NaI(Tl) detectors.

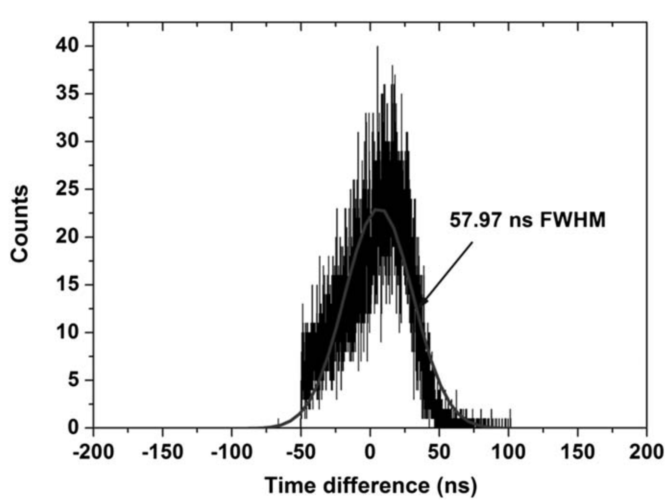

Fig. 7. Time difference distribution between DSSD and NaI(Tl) detector.

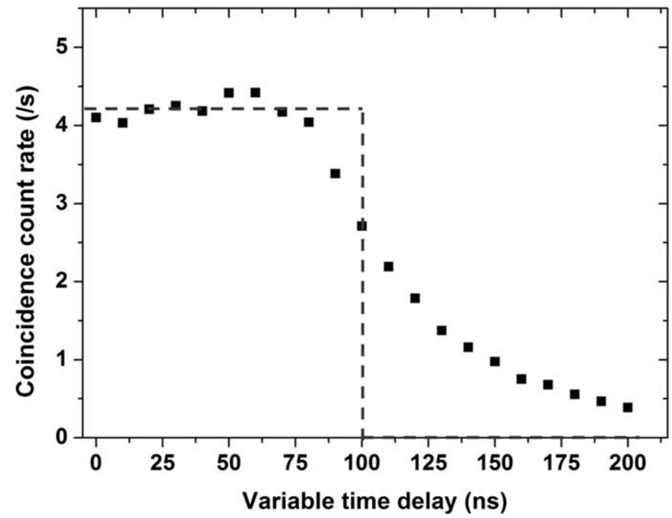

Fig. 8. Coincidence-delay curve measured with DSSD and NaI(Tl) detector. The dotted straight line represents the ideal case, that is, perfect timing resolution without any random coincidence events.

Fig. 8 shows the coincidence-delay curve measured from the scattering geometry and DAQ logic described. The trigger signal of the NaI(Tl) detector was delayed with 10 ns intervals. The straight dotted line represents the ideal case, that is, perfect timing resolution without any random coincidence events. Considering the timing resolution of the component detectors, the input width of the trigger signal fed into the coincidence logic of 200 ns for the DSSD and 50 ns for the NaI(Tl) detector, which determines the coincidence resolving time, were deemed to be proper for Compton imaging. Although the chance coincidence rate increases with the coincidence resolving time, the resolving times were determined to be several factors larger than the timing resolution [25], mainly because, in Compton imaging, most chance coincidence events can easily be rejected by applying the sum energy gate.

3.2. Compton imaging of ^{22}Na gamma source

To take a Compton image, a total of 18,335 triple coincidence events were registered from 10 h of acquisition and, among them, 762 and 663 events were selected by applying the energy gates of 511 ± 51 and 1275 ± 127 keV, respectively. The imaging sensitivities for the 511 and 1275 keV gammas were calculated as 4.15×10^{-8} and 6.50×10^{-8}, respectively. When compared with a single-scattering-type Compton camera, the imaging sensitivity of the double-scattering Compton camera is relatively low; however, this problem can be addressed by employing a multiple number of detectors stacked in the axial direction and/or expanded in the planar direction, for each of the first and second scatterer detectors. Reconstructed Compton images are shown in Fig. 9. The imaging resolution was 9.0 and 4.8 mm FWHM for 511 and 1275 keV, respectively, which were fairly good considering the limitations of the detectors and DAQ electronics used in the present study. The angular resolutions were determined to be 8.6° and 5.7° for 511 and 1275 keV, respectively, from the ARM distributions (Fig. 10). Fig. 11 shows three-dimensional Compton images that clearly illustrate that the double-scattering Compton camera can image the three-dimensional location of a radiation source from a fixed position. The image quality, moreover, can be significantly improved by imaging the source from several different directions or locations [26].

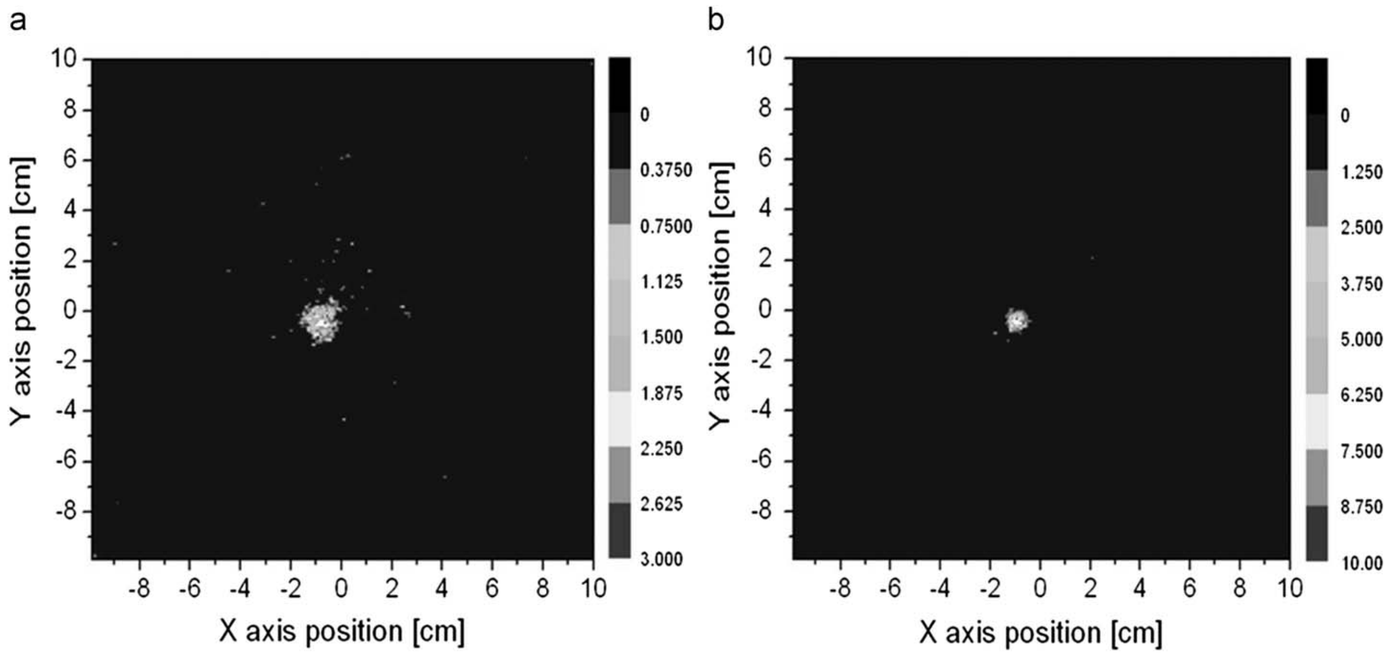

Fig. 9. Cross-sectional Compton images for 511 (left) and 1275 keV (right) gammas for a point-like (1 mm diameter) ^{22}Na check source.

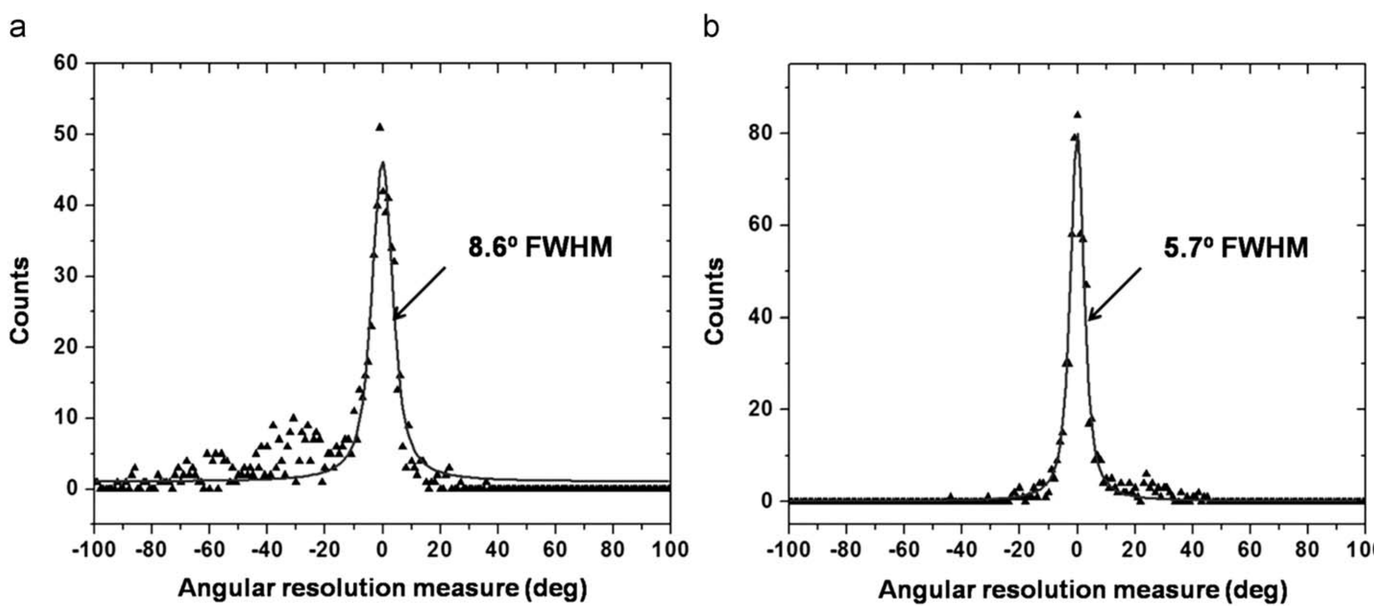

Fig. 10. Angular resolution measure (ARM) distributions for source energies of 511 (left) and 1275 keV (right).

4. Conclusions

In the present study, a double-scattering-type Compton camera was constructed as a proof-of-principle system for a compact high-resolution Compton camera, using two double-sided silicon strip detectors (DSSDs) and an NaI(Tl) absorber detector. The imaging resolution of the camera was 9.0 and 4.8 mm FWHM for 511 and 1275 keV, respectively, which were fairly good considering the limitations of the detectors and DAQ electronics used in the present study. Given the characteristics of the component detectors, it is believed that the double-scattering Compton camera can be developed as a very compact portable system (similar in size to a hand-held radiation survey meter) providing very high imaging resolution. The imaging resolution of the current system is not very high, but can be significantly improved by employing more sophisticated detectors and DAQ electronics. For example, the use of TTT3(DS)-500/1000 DSSDs (strip pitch = 760 μm; Micron Semiconductor, Sussex, UK) with a low-noise ASIC-based DAQ system, will dramatically improve the imaging resolution, by a factor of several times. The use of a higher-energy-resolution detector with better timing characteristics, such as an $LaBr_3$(Ce) scintillation detector, for the absorber detector, will also improve the imaging resolution of the Compton camera, specifically by applying a narrower sum-energy gate window and coincidence timing window, which results in rejecting more random coincidences. It should be noted that the enhancement of imaging resolution by employing the concept of double scattering in the scatter detectors does not change the inherent limitation of the Compton imaging resolution for low-energy photons imposed by the Doppler broadening effect and

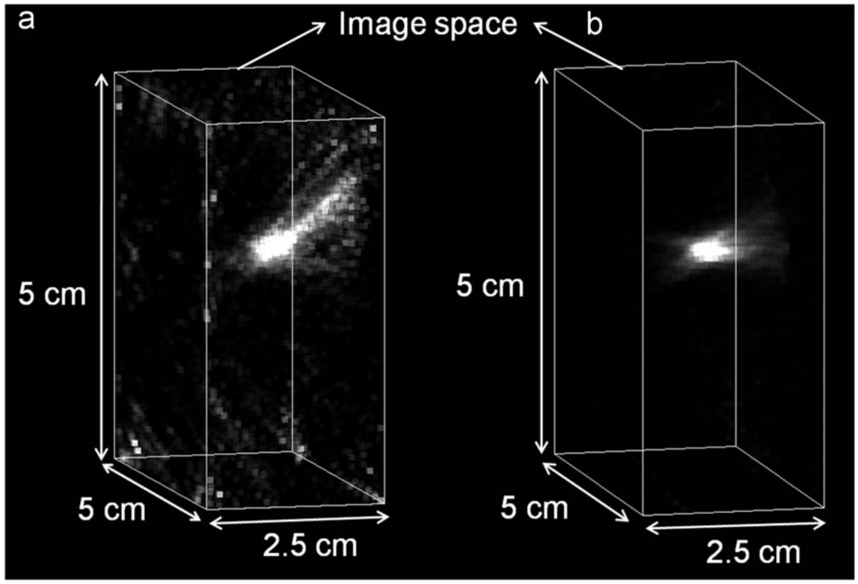

Fig. 11. Three-dimensional Compton images reconstructed using expectation-maximization algorithm in three-dimensional image space (5 cm × 5 cm × 2.5 cm) for the 511 (left) and 1275 keV (right) gammas.

limited energy resolutions of the component detectors. The concept of the double-scattering Compton camera is, therefore, more applicable to high-energy photon imaging (say, > a few hundred keV) in which the Doppler broadening effect is negligible and photon energy can be measured with relatively low uncertainty.

The current prototype system will be used to investigate the detailed characteristics of the double-scattering Compton camera knowledge of which is necessary for the development of a camera that offers both compactness and high-resolution. The current system will also be used to provide experimental data for the verification of our Monte Carlo simulations, which will be used to further optimize the camera.

For the very next step of our development, the first scatterer detector will be replaced with the TTT3(DS)-500, which is 10 cm × 10 cm × 0.05 cm and composed 128 strips on each side. To handle the multi-channel signals from the new DSSD, a low-noise ASIC-based DAQ system will be developed. Then, the double-scattering Compton camera will be tested for some practical applications that require high imaging resolution rather than high imaging sensitivity: for instances, (1) imaging of three-dimensional dose distribution in a dosimetric phantom for a proton beam therapy by measuring the distribution of the high-energy prompt gammas from proton interactions as a quality control purpose, and (2) imaging of the radioisotope distribution injected into an existing multiphase flow system in industrial process to determine the detailed flow patterns. In order to increase the imaging sensitivity of the double-scattering Compton camera, it is also considered to use many detectors for each of the first and second scatterer detectors. The scatterer detectors can be stacked in the axial direction and/or expanded in the planar direction to increase the imaging sensitivity. The use of 9 TTT3(DS)-500 detectors in planer direction and 5 detector layers in the axial direction for each of the first and second scatterer detectors will increase the imaging sensitivity by 3 or 4 orders of magnitude when compared with the current system. The imaging sensitivity will be also further increased by lowering the energy discrimination levels of the component detectors using the low-noise ASIC-based DAQ system.

Acknowledgement

This work was supported by the Nuclear R&D Program in Korea through BAERI and Basic Research program. One of the authors was supported by the Seoul Metropolitan Government through the Seoul Science Fellowship program.

References

[1] R.W. Todd, J.M. Nightingale, D.B. Everett, Nature 251 (1974) 132.
[2] V. Schoenfelder, et al., Astrophys. J. Suppl. Ser. 86 (1993) 657.
[3] G. Llosa, et al., IEEE Trans. Nucl. Sci. NS-55 (3) (2008) 936.
[4] S. Motomura, S. Enomoto, H. Haba, K. Igarashi, Y. Gono, Y. Yano, IEEE Trans. Nucl. Sci. NS-54 (3) (2007) 710.
[5] A.S. Hoover, R.M. Kippen, J.P. Sullivan, M.W. Rawool-Sullivan, W. Baird E.B. Sorensen, IEEE Trans. Nucl. Sci. NS-52 (6) (2005) 3047.
[6] S. Motomura, Y. Kanayama, H. Haba, K. Igarashi, Y. Watanabe, S. Enomoto, J. Anal. At. Spectrom. 23 (2008) 1089.
[7] J.H. Lee, N.Y. Kim, C.S. Lee, Z.H. Jang, Nucl. Phys. A 758 (2005) 150.
[8] K. Vetter, et al., Nucl. Instr. and Meth. A 579 (2007) 363.
[9] S. Watanabe, et al., IEEE Trans. Nucl. Sci. NS-52 (5) (2005) 2045.
[10] S.H. An, H. Seo, J.H. Lee, C.S. Lee, J.S. Lee, C.H. Kim, Nucl. Instr. and Meth. A 571 (2007) 251.
[11] H. Tajima, et al., IEEE Trans. Nucl. Sci. NS-52 (6) (2005) 2749.
[12] S. Takeda, et al., IEEE Trans. Nucl. Sci. NS-56 (3) (2009) 783.
[13] J.P. Sullivan, S.R. Tornga, M.W. Rawool-Sullivan, Appl. Radiat. Isot. 67 (2009) 617.
[14] M.G. Scannavini, R.D. Speller, G.J. Royle, I. Cullum, M. Raymond, G. Hall G. Iles, Nucl. Instr. and Meth. A 477 (2002) 514.
[15] T. Kamae, R. Enomoto, N. Hanada, Nucl. Instr. and Meth. A 260 (1987) 254.
[16] E.C. Bellm, et al., IEEE Trans. Nucl. Sci. NS-56 (3) (2009) 1250.
[17] A. Zoglauer, G. Kanbach, Proc. SPIE-Int. Soc. Opt. Eng. 4851 (2003) 1302.
[18] R. Brun, F. Rademakers, Nucl. Instr. and Meth. A 389 (1997) 81.
[19] S.J. Wilderman, J.A. Fessler, N.H. Clinthorne, J.W. LeBlanc, W.L. Rogers, IEEE Trans. Nucl. Sci. NS-48 (2001) 111.
[20] T. Hebert, R. Leahy, M. Singh, J. Opt. Soc. Am. A 7 (1990) 1305.
[21] S.M. Kim, J.S. Lee, M.N. Lee, J.H. Lee, C.S. Lee, C.H. Kim, D.S. Lee, S.J. Lee, Nucl. Instr. and Meth. A 571 (2007) 255.
[22] M.E. Bandstra, et al., IEEE Nucl. Sci. Symp. Conf. Rec. 2 (2006) 770.
[23] S. Takeda, et al., Proc. SPIE 6706 (2007) 67060S.
[24] J.J. Olivero, R.L. Longbothum, J. Quant. Spectrosc. Radiat. Transfer 17 (1997) 233.
[25] G.F. Knoll, Radiation Detection and Measurement, 3rd ed., John Wiley and Sons, New York, 2000, pp. 665.
[26] R. Kohara, et al., IEEE Nucl. Sci. Symp. Conf. Rec. (2008) 3906.